Pergamon

Int. J. Heat Mass Transfer. Vol. 39, No. 16, pp. 3425–3430, 1996

0017-9310/96 $15.00+0.00

0017-9310(95)00406-8

The effect of inertia on free convection from a horizontal surface embedded in a porous medium

D. A. S. REES

School of Mechanical Engineering, University of Bath, Claverton Down, Bath BA2 7AY, U.K.

(*Received* 14 *June* 1994 *and in final form* 17 *November* 1995)

Abstract—It is well-known that the effect of inertia on the free convection boundary layer flow induced by a uniformly heated horizontal surface in a porous medium is weak, and modifies the heat transfer characteristics at second-order. In this paper we consider the case where the inertia effects are sufficiently large that the leading-order boundary layer theory is modified; this is equivalent to reconsidering flow sufficiently near to the leading edge that the induced velocities are large enough for inertia effects to arise, but sufficiently far from the leading edge that the boundary layer approximation remains valid. The resulting nonsimilar boundary layer equations are solved using the Keller-box method. Near the leading edge inertia effects are found to dominate, but Darcy-flow is re-established further downstream. Copyright © 1996 Elsevier Science Ltd.

1. INTRODUCTION

Natural convection within fluid-saturated porous media has attracted considerable attention in the last three decades because of its importance in geophysics, oil recovery techniques, thermal insulation engineering, packed-bed catalytic reactors and heat storage beds. A number of similarity solutions and numerical studies of natural convection in porous media have been presented. A comprehensive review of relevant papers may be found in the recent monograph by Nield and Bejan [1]. Most of the studies included there refer to configurations where Darcy's law is valid. However, this law is known to be valid only for relatively slow flows through the porous matrix. In general, we must consider the effect of the fluid inertia, as well as viscous diffusion at boundaries which may well become significant for materials with very high porosities, such as fibrous media and foams.

In this paper we consider the effect of fluid inertia on the boundary layer flow induced by an upward-facing uniformly heated horizontal surface embedded in a porous medium. The first study to deal with the horizontal plate problem was undertaken by Cheng and Chang [2], who assumed that Darcy's law applied. They also assumed that the boundary layer approximation applied, which is equivalent to setting the Darcy–Rayleigh number, Ra, to an asymptotically large value. Under these conditions the resulting boundary layer equations admit similarity solutions for the flow and temperature profiles. This analysis was extended later by Riley and Rees [3] who used the method of matched asymptotic expansions to obtain a more accurate solution.

In ref. [3], the authors also investigated the effect of fluid inertia by including the nonlinear Ergun [4] model in the Darcy law formulation. The same model was also employed by Plumb and Huenefeld [5], Vasantha *et al.* [6] and Lai and Kulacki [7]. The one aspect of the analysis of ref. [3] which is of interest here, and indeed motivates the present study, is that, for the horizontal plate, fluid inertia has only a weak effect on the flow, since the modification to the standard Darcy law theory arises at second-order in the asymptotic theory. This fact may be explained by considering the strength of the induced flowfield, which is weak compared with the equivalent inclined or vertical configurations for which non-Darcy effects appear at leading order. Thus, the fluid inertia is relatively unimportant at leading order for the horizontal surface. However, this statement can only be considered to be true for distances sufficiently far from the leading edge. In the analysis of ref. [3], the slip velocity of the fluid on the horizontal surface varies as $x^{-1/3}$ at leading order, where x is a nondimensional distance from the leading edge. Therefore, it is quite possible that when x is sufficiently small, the slip velocity can be sufficiently large that inertia effects can influence even the leading-order profiles. An alternative scenario, one that we shall use here, is to consider sufficiently large values of what we shall term the Darcy–Grashof number, Gr, a nondimensional measure of the strength of the inertia effects. Riley and Rees [3] considered values which were $O(1)$ as $Ra \to \infty$. Here, we show that inertia forces are non-negligible at leading order when $Gr = O(Ra^{1/3})$. Although the resulting flow is nonsimilar, it is, somewhat surprisingly, independent of the size of $GrRa^{-1/3}$. We present the boundary layer analysis in Section 2 and the results in Section 3. We conclude with a brief discussion in Section 4.

NOMENCLATURE

a, b	constants
d	particle or pore diameter
f, F	reduced streamfunctions
g	acceleration due to gravity
Gr	Darcy–Grashof number
k_e	effective thermal conductivity
K	permeability
$\tilde{K}$	inertial parameter
l	macroscopic lengthscale
p	pressure
q	rate of heat flux
Q	nondimensional velocity; see equation (11)
Ra	Darcy–Rayleigh number based on l
T	dimensional temperature
u, v	fluid velocities in the x- and y-directions, respectively
$\mathbf{u} = (u, v)$	velocity vector
x, y	streamwise and cross-stream Cartesian coordinates.

Greek symbols

α	measure of the strength of inertia effects, see equation (16)
β	coefficient of thermal expansion
ε	porosity
ξ, η	pseudo-similarity variables
χ, ζ	pseudo-similarity variables
κ	thermal diffusivity of the porous medium
θ	dimensionless temperature
μ	dynamic viscosity
ρ	density
ψ	streamfunction.

Superscripts

*	dimensional variables
–	transformed variables
^	transformed variables.

Subscripts

G	global
L	local
w	condition at the wall
ref	reference value
∞	condition at infinity.

2. GOVERNING EQUATIONS AND BOUNDARY LAYER ANALYSIS

We consider a horizontal surface which is embedded in a homogeneous fluid-saturated porous medium. The surface is held at the constant temperature, T_w, whilst the ambient temperature of the medium is T_∞. We assume that $T_w > T_\infty$ and examine the resulting two-dimensional flow induced by buoyancy forces in the medium along the surface. We take as our governing equations,

$$u^*_{x^*} + v^*_{y^*} = 0 \tag{1}$$

$$\left(1 + \frac{\tilde{K}}{\mu}|\mathbf{u}^*|\right)u^* = -\frac{K}{\mu}p^*_{x^*} \tag{2}$$

$$\left(1 + \frac{\tilde{K}}{\mu}|\mathbf{u}^*|\right)v^* = -\frac{K}{\mu}(p^*_{y^*} - \rho g\beta(T - T_\infty)) \tag{3}$$

$$u^*T_{x^*} + v^*T_{y^*} = \kappa(T_{x^*x^*} + T_{y^*y^*}) \tag{4}$$

(see ref. [3]) where Darcy's law is recovered when $\tilde{K} = 0$. In equations (1)–(4) x^* and y^* are the Cartesian coordinates along and perpendicular to the heated plate, respectively, u^* and v^* are the respective fluid velocity fluxes, p is the dynamic pressure and T is the temperature. Furthermore, K is the permeability of the porous medium, $\tilde{K}$ is a material parameter which may be thought of as a measure of the inertial impedance of the matrix, g is the acceleration due to gravity, ρ the fluid density, μ the dynamic viscosity, β the coefficient of cubical expansion of the fluid and κ the effective thermal diffusivity of the saturated medium. To illustrate how the additional nonlinear term comes into play when the porosity is high we quote Ergun's relations for K and $\tilde{K}$,

$$K = \frac{d^2\varepsilon^3}{150(1-\varepsilon)^2} \quad \tilde{K} = \frac{1.75d}{150(1-\varepsilon)} \tag{5}$$

(see ref. [4]) where ε denotes the porosity, and d is the characteristic pore or particle diameter. Clearly, when $\varepsilon \sim 1$ then $\tilde{K}$ is large and the nonlinear term is important.

Equations (1)–(4) may be nondimensionalized by introducing the substitutions

$$(x^*, y^*) = l(x, y), \quad (u^*, v^*) = \frac{\kappa}{l}(u, v) \tag{6a,b}$$

$$p^* = \frac{\kappa\mu}{K}p \quad T = T_\infty + (T_w - T_\infty)\theta \tag{6c,d}$$

where l is a macroscopic lengthscale. If, in addition, we introduce the two-dimensional streamfunction using

$$(u, v) = (\psi_y, -\psi_x) \tag{7}$$

then we obtain the equations,

$$(1 + GrQ/Ra)\nabla^2\psi + (Gr/QRa)(\psi_x^2\psi_{xx} + 2\psi_x\psi_y\psi_{xy} + \psi_y^2\psi_{yy}) = -Ra\theta_x \tag{8}$$

$$\nabla^2\theta = \psi_y\theta_x - \psi_x\theta_y. \tag{9}$$

In equations (8) and (9) the Darcy–Rayleigh number, Ra, and the Darcy–Grashof number, Gr, are given by

$$Ra = \frac{\rho g\beta(T_w - T_\infty)lK}{\kappa\mu} \quad Gr = \left(\frac{\rho}{\mu}\right)^2 K\tilde{K}g\beta(T_w - T_\infty) \tag{10a,b}$$

and the term Q is a fluid flux given by

$$Q^2 = \psi_x^2 + \psi_y^2. \tag{11}$$

If we assume that $x = O(1)$ as $Ra \to \infty$, then the boundary layer approximation is valid when $y \ll 1$. Subject to this approximation equations (8) and (9) reduce to

$$(1 + 2|\psi_y|GrRa^{-1})\psi_{yy} = -Ra\theta_x, \tag{12}$$

$$\theta_{yy} = \psi_y\theta_x - \psi_x\theta_y, \tag{13}$$

and are subject to the boundary conditions,

$$\psi = 0 \quad \theta = 1 \quad \text{on } y = 0 \tag{14}$$

$$\frac{\partial\psi}{\partial y} \to 0 \quad \theta \to 0 \quad \text{as } y \to \infty. \tag{15}$$

In ref. [3], the Darcy–Grashof number was taken to be $O(1)$ as $Ra \to \infty$, and, given the standard Darcy law boundary layer scalings, $\psi = O(Ra^{1/3})$ and $y = O(Ra^{-1/3})$, the inertia term in equation (12), namely $2|\psi_y|GrRa^{-1}$, is formally negligible as $Ra \to \infty$. However, if $Gr = O(Ra^{1/3})$, then the inertia term remains significant. Therefore we introduce the following rescalings:

$$\psi = Ra^{1/3}\hat{\psi} \quad y = Ra^{-1/3}\hat{y} \quad x = \hat{x} \quad \text{and} \quad Gr = \alpha Ra^{1/3} \tag{16}$$

in equations (12) and (13). Here, α is a constant which measures the strength of the fluid inertia. We obtain the following equations:

$$(1 + 2\alpha\hat{\psi}_{\hat{y}})\hat{\psi}_{\hat{y}\hat{y}} = -\theta_{\hat{x}} \tag{17}$$

$$\theta_{\hat{y}\hat{y}} = \hat{\psi}_{\hat{y}}\theta_{\hat{x}} - \hat{\psi}_{\hat{x}}\theta_{\hat{y}} \tag{18}$$

in which we have dropped the modulus sign from the inertia term, since the function $\hat{\psi}_{\hat{y}}$ will always turn out to be positive.

The constant, α, can be scaled out of the equations by introducing the transformation

$$\hat{\psi} = \alpha^{1/4}\bar{\psi}, \quad \hat{x} = \alpha^{3/4}\bar{x}, \quad \hat{y} = \alpha^{1/2}\bar{y}; \tag{19}$$

now equations (17) and (18) become,

$$(1 + 2\bar{\psi}_{\bar{y}})\bar{\psi}_{\bar{y}\bar{y}} = -\theta_{\bar{x}} \tag{20}$$

$$\theta_{\bar{y}\bar{y}} = \bar{\psi}_{\bar{y}}\theta_{\bar{x}} - \bar{\psi}_{\bar{x}}\theta_{\bar{y}}. \tag{21}$$

A third transformation is introduced which defines the set of pseudo-similarity variables, (ξ, η), which, in the absence of inertia effects, correspond precisely to the similarity variables used in ref. [3]

$$\bar{\psi} = \xi f(\xi, \eta) \quad \theta = \theta(\xi, \eta) \tag{22}$$

$$\xi = \bar{x}^{1/3} \quad \eta = \bar{y}/\bar{x}^{2/3}. \tag{23}$$

Equations (20) and (21) reduce to the form

$$(\xi + 2f_\eta)f_{\eta\eta} = \xi(\tfrac{2}{3}\eta\theta_\eta - \tfrac{1}{3}\xi\theta_\xi), \tag{24}$$

$$\theta_{\eta\eta} + \tfrac{1}{3}f\theta_\eta = \tfrac{1}{3}\xi(f_\eta\theta_\xi - f_\xi\theta_\eta) \tag{25}$$

and the boundary conditions become

$$f = 0 \quad \theta = 1 \quad \text{on } \eta = 0 \quad \text{and} \quad f_\eta, \theta \to 0 \quad \text{as} \quad \eta \to \infty. \tag{26}$$

This set of nonsimilar boundary layer equations may be solved easily using the Keller-box method for moderate and large values of ξ. However, when ξ is close to or equal to zero we have to introduce a further transformation since, in terms of η, the boundary layer thickness may be shown to be infinite at $\xi = 0$. Hence, we define a second set of pseudo-similarity variables, (χ, ζ), according to

$$f = \chi F(\chi, \zeta) \quad \theta = \theta(\chi, \zeta) \tag{27}$$

$$\chi = \xi^{1/5} \quad \zeta = \eta\xi^{1/5}. \tag{28}$$

Equations (24) and (25) become

$$(\chi^3 + 2F_\zeta)F_{\zeta\zeta} = \tfrac{3}{5}\zeta\theta_\zeta - \tfrac{1}{15}\chi\theta_\chi \tag{29}$$

$$\theta_{\zeta\zeta} + (\tfrac{1}{3} + \tfrac{1}{15}\chi^2)F\theta_\zeta = \tfrac{1}{15}\chi(F_\zeta\theta_\chi - F_\chi\theta_\zeta) \tag{30}$$

which may be solved using the Keller-box method, since the boundary layer has finite thickness at $\chi = 0$ using these variables. The boundary conditions are,

$$F = 0 \quad \theta = 1 \quad \text{on } \zeta = 0 \quad \text{and} \quad F_\zeta, \quad \theta \to 0 \quad \text{as } \zeta \to \infty. \tag{31}$$

Finally, it may be helpful to write the variables x, y and ψ, defined in equation (16), in terms of the two sets of pseudo-similarity variables defined in equations (22), (23) and (27), (28):

$$x = \alpha^{3/4}\xi^3 \quad y = Ra^{-1/3}\alpha^{1/2}\eta\xi^2 \quad \psi = Ra^{1/3}\alpha^{1/4}\xi f(\xi, \eta) \tag{32}$$

and

$$x = \alpha^{3/4}\chi^{15} \quad y = Ra^{-1/3}\alpha^{1/2}\zeta\chi^9 \quad \psi = Ra^{1/3}\alpha^{1/4}\chi^6 F(\chi, \zeta). \tag{33}$$

In turn, the variables ζ and η are given by

$$\zeta = \frac{yRa^{1/3}}{\alpha^{1/20}x^{3/5}} \quad \eta = \frac{yRa^{1/3}}{x^{2/3}}. \tag{34,35}$$

3. RESULTS AND DISCUSSION

Equations (24) and (25) and equations (29) and (30) were solved numerically using the Keller-box method (see ref. [8]). The former pair were solved over the interval $0 \leqslant \chi \leqslant 1$, while the latter were solved on a nonuniform grid in the interval $1 \leqslant \xi \leqslant 10000$. In the cross-stream direction a nonuniform grid of 131 points was used over the range $0 \leqslant \eta, \zeta \leqslant 50$. At each streamwise station convergence to the solution of the nonlinear governing equations was deemed to have occurred when the maximum pointwise change in successive Newton–Raphson iterates was less than 10^{-8}; this generally occurred after three or four iterations. The solution of equations (28) and (29) at $\chi = 0$, that is, the ordinary differential equations,

$$2F_\zeta F_{\zeta\zeta} = \tfrac{3}{5}\zeta\theta_\zeta \tag{36}$$

$$\theta_{\zeta\zeta} + \tfrac{1}{3}F\theta_\zeta = 0 \tag{37}$$

subject to the boundary conditions, (30) presented much greater difficulties since, for large values of ζ, the coefficient of $F_{\zeta\zeta}$ is exponentially small. Indeed, it is a very straightforward analysis to show that, if $F \to a$, a constant, as $\zeta \to \infty$ when $\chi = 0$, then

$$\theta \sim b\mathrm{e}^{-a\zeta/3} \quad \text{and} \quad F_\zeta \sim (\tfrac{3}{5}b\zeta)^{1/2}\mathrm{e}^{a\zeta/6} \tag{38}$$

where b is also a constant. A satisfactory approach to the numerical solution at $\chi = 0$ was obtained by using a suitable initial iterate and iterating with under-relaxation in order that numerical values of F_ζ remain positive over the whole range of integration for all iterates. The inertia-dominated profiles thus obtained are depicted in Fig. 1. We note, for reference, that

$$\theta_\zeta(\zeta = 0) = -0.4282\,, \quad F_\zeta(\zeta = 0) = 0.9624$$

$$\text{and} \quad F(\zeta) \to 3.6124 \quad \text{as } \zeta \to \infty. \tag{39}$$

The local rate of heat transfer, q_L, is given by

$$q_L = -\frac{k_c(T_w - T_\infty)}{l}\frac{\partial\theta}{\partial y}(y = 0) \tag{40}$$

where

$$\frac{\partial\theta}{\partial y} = \frac{Ra^{1/3}\theta_\zeta}{\alpha^{1/2}\xi^{9/5}} \quad \text{when } \xi \leqslant 1 \tag{41a}$$

$$= \frac{Ra^{1/3}\theta_\eta}{\alpha^{1/2}\xi^2} \quad \text{when } \xi \geqslant 1 \tag{41b}$$

at either $\zeta = 0$ or $\eta = 0$. Local heat transfer results are presented in Fig. 2 in the forms

(i) θ_ζ for $\xi \leqslant 1$ and $\xi^{1/5}\theta_\eta$ for $\xi \geqslant 1$, and

(ii) $\xi^{1/5}\theta_\zeta$ for $\xi \leqslant 1$ and θ_η for $\xi \geqslant 1$.

Both graphs are plotted against $\xi = x^{1/3}/\alpha^{1/4}$. The first form displays clearly the behaviour of the local rate of heat transfer for small values of ξ, where non-Darcy effects dominate, whereas the second form shows the approach to the Darcy flow limit as $\xi \to \infty$.

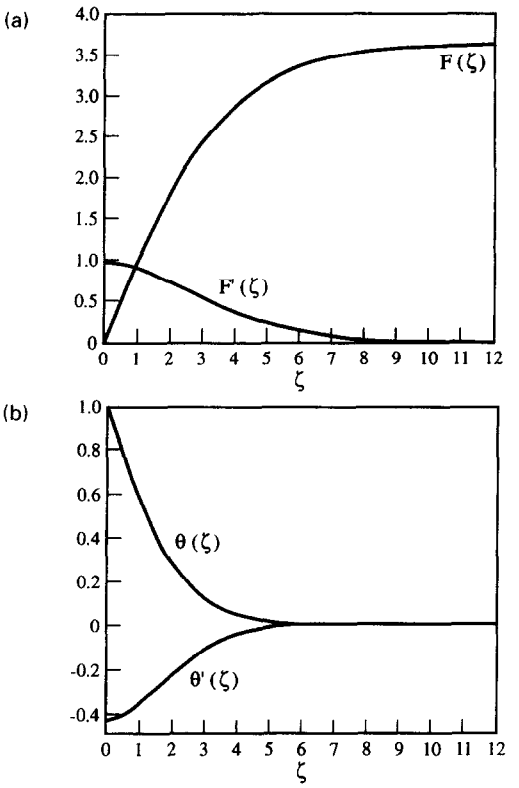

Fig. 1. Inertia-dominated profiles, (a) $F(\zeta)$ and $F_\zeta(\zeta)$, (b) $\theta(\zeta)$ and $\theta_\zeta(\zeta)$.

The global rate of heat transfer, q_G, is given by

$$q_G = -k_c(T_w - T_\infty)\int_0^{x_{ref}} \frac{\partial\theta}{\partial y}(x, y = 0)\,\mathrm{d}x. \tag{42}$$

In terms of the pseudo-similarity variables, this becomes

$$q_G = -k_c(T_w - T_\infty)Ra^{1/3}\alpha^{1/4} \times \int_0^{\chi_{ref}} 15\chi^5\theta_\zeta(\chi, \zeta = 0)\,\mathrm{d}\chi \quad \text{when } \xi \leqslant 1 \tag{43a}$$

$$= -k_c(T_w - T_\infty)Ra^{1/3}\alpha^{1/4}$$

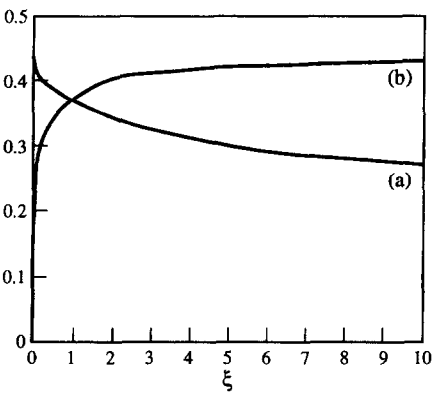

Fig. 2. Local rates of heat transfer as a function of ξ: (a) $\alpha^{1/2}Ra^{-1/3}\xi^{9/5}(\partial\theta/\partial y)(\xi, 0)$, (b) $\alpha^{1/2}Ra^{-1/3}\xi^2(\partial\theta/\partial y)(\xi, 0)$.

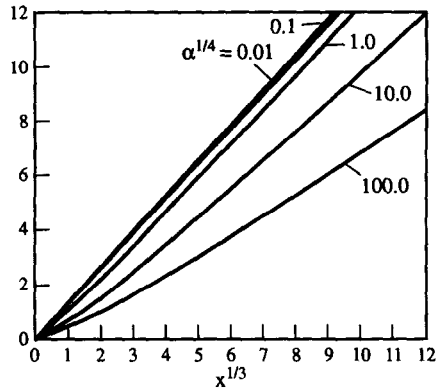

Fig. 3. Scaled global rates of heat transfer, $-q_G/[k_c(T_w - T_\infty)Ra^{1/3}\alpha^{1/4}]$, as a function of $x^{1/3} = \alpha^{1/4}\xi$, for $\alpha = 0.01, 0.1, 1.0, 10.0$ and 100.0.

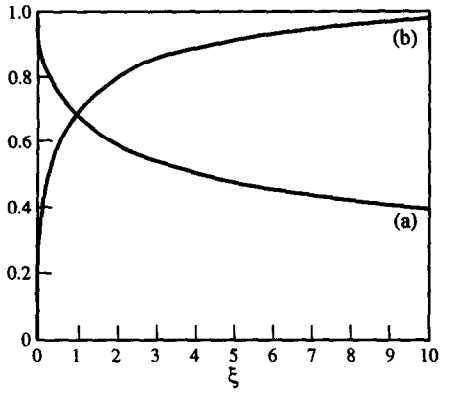

Fig. 4. Local slip-velocity as a function of ξ : (a) $\alpha^{1/4}Ra^{-2/3}\xi^{3/5}(\partial\psi/\partial y)(\xi, 0)$, (b) $\alpha^{1/4}Ra^{-2/3}\xi\ (\partial\psi/\partial y)(\xi, 0)$.

$$\times \int_0^{\xi_{\text{ref}}} 3\theta_\eta(\xi, \eta = 0)\, d\xi \quad \text{when } \xi \geqslant 1. \quad (43b)$$

In Fig. 3 we display q_G as a function of $x_{\text{ref}}^{1/3}$ for various values of α, where it should be noted that, in view of the transformation (19), only one computation is necessary; graphs for different values of α are obtained by a suitable rescaling. When $\alpha = 0$, the Darcy flow case is recovered and q_G is a linear function of $x_{\text{ref}}^{1/3}$. As α increases, the region over which the inertia effects modify the Darcy-flow profiles becomes larger, but it always includes the leading edge. The presence of inertial forces causes an increased boundary layer thickness near the leading edge compared with the Darcy flow case [cf. the definitions of ζ and η in equations (34) and (35), respectively] and this, in turn, reduces the global rate of heat transfer as α increases.

Due to the absence of boundary effects in the model we have used here, there is a wall slip-velocity. In nondimensional terms the slip-velocity is given by

$$\psi_y = \frac{Ra^{2/3}}{\alpha^{1/4}\xi^{3/5}} F_\zeta(\chi, \zeta = 0), \quad (\xi \leqslant 1), \quad (44a)$$

$$= \frac{Ra^{2/3}}{\alpha^{1/4}\xi} f_\eta(\xi, \eta = 0), \quad (\xi \geqslant 1). \quad (44b)$$

Figure 4 displays the slip-velocity, again in two forms

(i) F_ζ for $\xi \leqslant 1$ and $\xi^{-2/5} f_\eta$ for $\xi \geqslant 1$ and

(ii) $\xi^{2/5} F_\zeta$ for $\xi \leqslant 1$ and f_η for $\xi \geqslant 1$.

The first form allows us to see clearly the behaviour of the slip-velocity in the strongly non-Darcy region near the leading edge. The second shows the diminishing effect of inertia at increasing distances from the leading edge.

4. CONCLUSIONS

We have investigated how the presence of inertia modifies the flow and heat transfer from a horizontal heated surface in porous media. This has been achieved by assuming that the Darcy–Grashof number is sufficiently large that fluid-inertia terms enter the boundary layer equations at leading order, rather than at higher orders as is the case in ref. [3]. More specifically, we have taken $Gr = O(Ra^{1/3})$ as $Ra \to \infty$.

Inertia effects are found to dominate the flow near the leading edge, but become progressively weaker at increasingly large distances from the leading edge. Eventually the well-known Darcy-flow profiles are recovered.

Although the presence of fluid inertia serves to decrease both the local rate of heat transfer and the slip-velocity near to the leading edge, it is insufficient to stop these quantities becoming infinite as $x \to 0^+$ [cf. equations (41a) and (44a)]. However, the strength of the singularity is reduced: as $x \to 0^+$ the local rate of heat transfer becomes proportional to $x^{-3/5}$ as compared with $x^{-2/3}$ for Darcy flow, and the local slip-velocity becomes proportional to $x^{-1/5}$ as compared with $x^{-1/3}$ for Darcy flow. It might be conjectured that a detailed analysis of the region sufficiently close to the leading edge, where the governing equations are fully elliptical, could yield a rate of heat transfer and a slip-velocity which are finite, and which would be matched asymptotically onto our present solutions. However, the exact solutions for Darcy flow given in ref. [9] show that the strength of singularity at the origin depends ultimately on the angle between the heated surface and a second bounding surface.

REFERENCES

1. D. A. Nield and A. Bejan, *Convection in Porous Media*. Springer, Berlin (1992).
2. P. Cheng and I. D. Chang, On buoyancy induced flows in a saturated porous medium adjacent to impermeable horizontal surfaces, *Int. J. Heat Mass Transfer* **19**, 1267–1272 (1976).
3. D. S. Riley and D. A. S. Rees, Non-Darcy natural con-

vection from arbitrarily inclined heated surfaces in saturated porous media, *Q. J. Mech. Appl. Math.* **38,** 277–295 (1985).
4. S. Ergun, Fluid flow through packed columns, *Chem. Engng Proc.* **48,** 89–94 (1952).
5. O. A. Plumb and J. C. Huenefeld, Non-Darcy natural convection from heated surfaces in saturated porous media, *Int. J. Heat Mass Transfer* **24,** 765–768 (1981).
6. R. Vasantha, I. Pop and G. Nath, Non-Darcy natural convection over a slender vertical frustrum of a cone in a saturated porous medium, *Int. J. Heat Mass Transfer* **29,** 153–156 (1986).
7. F. C. Lai and F. A. Kulacki, Non-Darcy convection from horizontal impermeable surfaces in saturated porous media, *Int. J. Heat Mass Transfer* **30,** 2189–2192 (1987).
8. H. B. Keller and T. Cebeci, Accurate numerical methods for boundary layer flows—I. Two-dimensional flows, *Proceedings of the International Conference on Numerical Methods in Fluid Dynamics, Lecture Notes in Physics.* Springer, New York (1971).
9. D. A. S. Rees and A. P. Bassom, Some exact solutions for free convective flows over heated semi-infinite surfaces in porous media, *Int. J. Heat Mass Transfer* **34,** 1564–1567 (1991).